We are IntechOpen,
the world's leading publisher of
Open Access books
Built by scientists, for scientists

6,900
Open access books available

185,000
International authors and editors

200M
Downloads

154
Countries delivered to

Our authors are among the

TOP 1%
most cited scientists

12.2%
Contributors from top 500 universities

BOOK CITATION INDEX
CLARIVATE ANALYTICS
INDEXED

WEB OF SCIENCE™

Selection of our books indexed in the Book Citation Index
in Web of Science™ Core Collection (BKCI)

Interested in publishing with us?
Contact book.department@intechopen.com

First Principles Study of
Si/Ge Core-Shell Nanowires
- Structural and Electronic Properties

Xihong Peng[1], Fu Tang[2] and Paul Logan[2]
[1]Department of Applied Sciences and Mathematics, Arizona State University, Mesa,
[2]Department of Physics, Arizona State University, Tempe,
USA

1. Introduction

One-dimensional semiconductor nanostructures, such as Si and Ge nanowires, have attracted extensive research efforts over the past decades (B. Y-K Hu & Das Sarma, 1992; Hirschman et al., 1996; Morales & Lieber, 1998; Holmes et al., 2000; Cui & Lieber, 2001; Cui et al., 2001, 2003; Koo et al., 2004; Audoit et al., 2005; X. Y. Wu et al., 2008; Dailey & Drucker, 2009). They are expected to play important roles as both interconnects and functional components in future nanoscale electronic and optical devices, such as light-emitting diodes (LEDs) (Hirschman et al., 1996; Cui & Lieber, 2001), ballistic field-effect transistors (FETs) (Cui et al., 2003; Koo et al., 2004), inverters (Cui & Lieber, 2001), and nanoscale sensors (Cui et al., 2001; Hahm & Lieber, 2004). Experimental and theoretical investigations showed that in these nanoscale structures charge carriers are confined in the lateral direction of the wires, thus quantum confinement effect is expected to play an important role on the electronic properties. This confinement effect has been observed, for example, in photoluminescence studies, by exhibiting substantial blue-shift of emission with reduction of the nanowire diameter (Z. Wu et al., 2008; Beckman et al., 2006; Bruno et al., 2005). Researchers also found that the band gap of Si and Ge nanowires depends on several factors, such as size (Beckman et al., 2006; Bruno et al., 2005; Arantes & Fazzio, 2007), crystalline orientation (Bruno et al., 2005; Arantes & Fazzio, 2007; Medaboina et al., 2007), surface chemistry (Medaboina et al., 2007; Kagimura et al., 2007), and doping (Medaboina et al., 2007; Peelaers et al., 2007).

Recently, particular attention has been given to Si/Ge core-shell nanowires, in which factors, such as heterostructure composition and interface geometry, can be further manipulated to tune the electronic properties of nanowires (Kagimura et al., 2007; Lauhon et al., 2002; Y. Y. Wu et al., 2002; Lu et al., 2005; Trammell et al., 2008; J. Q. Hu et al., 2009; Peng & Logan, 2010; Peng et al., 2011b). Compared to pure Si and Ge wires, the core-shell structure has some greater properties. For instance, a better conductance and higher mobility of charge carries can be obtained, due to the conduction and valence band offsets in the core-shell nanowires (Kagimura et al., 2007; Goldthorpe et al., 2008; L. Yang et al., 2008). The band offsets also offer the heterostructure a wide range of applications in solar cells (Tian et al., 2007) and high-switching speed transistors (Y. J. Hu et al., 2008).

Experimentally, Yang and colleagues (J. E. Yang et al. 2006) grew crystalline $Si_{1-x}Ge_x$ nanowires by an Au catalyst-assisted chemical vapor synthesis, and showed that the energy gap of the $Si_{1-x}Ge_x$ nanowires can be tuned in the range from near-infrared to visible regions. In addition, Varahramyan and co-worker (Varahramyan et al., 2009) used ultrahigh vacuum chemical vapor deposition to grow Si_xGe_{1-x} epitaxial core-shell nanowires, and the Si/Ge shell content can be tuned to enable radial band and strain engineering in these heterostructures.

In addition to the experimental studies, several theoretical calculations were performed to study the quantum confinement effect in Si/Ge core-shell nanowires (Amato et al., 2009; Musin & Wang, 2005, 2006; L. Yang et al., 2008). In these calculations, the band gap and near-gap electronic states are particularly investigated as a function of hetero-composition. For example, Wang's group (Musin & Wang, 2005, 2006) reported the band gap of Si/Ge core-shell nanowires as a function of composition for wires with diameter up to 3 nm; Migas & Borisenko (Migas & Borisenko, 2007) studied the electronic properties of Si/Ge core-shell nanowire along the [100] direction with a diameter of 1.5 nm; Yang et al. (L. Yang et al., 2008) investigated the near-gap electronic states with the core and shell regions along [110] and [111] directions with diameter up to 4 nm.

Our group (Peng & Logan, 2010; Peng et al., 2011b), in particular, explored the effect of intrinsic and external strain on the band structures of Si/Ge core-shell nanowires along the [110] direction with the wire diameter up to 5 nm. It is known that strain is used as a routine parameter in industry to engineer electronic properties, such as the band gap, of semiconductors. In the Si/Ge core-shell nanowires, there is an intrinsic strain in the core-shell interface, due to the lattice mismatch between Si and Ge (Hahm & Lieber, 2004). In addition, external strain can be also applied to engineer the band structures. There are a few limited experimental studies in synthesis, strain relaxation, and equilibrium strain-energy analysis of coherently strained Si/Ge core-shell nanowires (Goldthorpel et al., 2008; Trammell et al., 2008). Here, we reported a detailed theoretical study of the effects of both intrinsic and external strains on the structural, mechanical, and electronic properties of Si/Ge core-shell nanowires.

We found that the intrinsic strain in the core-shell nanowires has significantly countered the quantum confinement effect and reduced the band gap of the core-shell nanowires. In addition, external uniaxial strain can further modulate the bands structure of the core-shell nanowires. Therefore, electronic properties, such as the gap, effective masses of charge carriers and work function, are substantially tuned by the strain.

2. Methods

First principles density-functional theory (DFT) (Kohn & Sham, 1965) calculations were performed to study Si/Ge core-shell nanowires. The simulations were done using local density approximation (LDA) implemented in Vienna Ab-initio Simulation Package (Kresse & Furthmuller, 1996a, 1996b). A pseudo-potential plane wave method was used and the plane wave energy cutoff for the wave-function basis is set to be 200.0 eV. Core electrons were described using ultra-soft Vanderbilt pseudo-potentials (Vanderbilt, 1990). Reciprocal space was sampled at $1 \times 1 \times 4$ K-points using Monkhorst Pack mesh. A larger plane wave energy cutoff of 350.0 eV and a K-points mesh of $1 \times 1 \times 9$ were used to check the calculations. No significant difference was found in the results using those parameters and the current setting. In the band structure calculations, 21 K-points were scanned along the reciprocal direction from Γ to X.

(a) 2.5 nm-Core$_{30}$Shell$_{46}$H$_{28}$ (b) 3.7 nm-Core$_{30}$Shell$_{142}$H$_{44}$ (c) 4.7 nm-Core$_{30}$Shell$_{246}$H$_{52}$
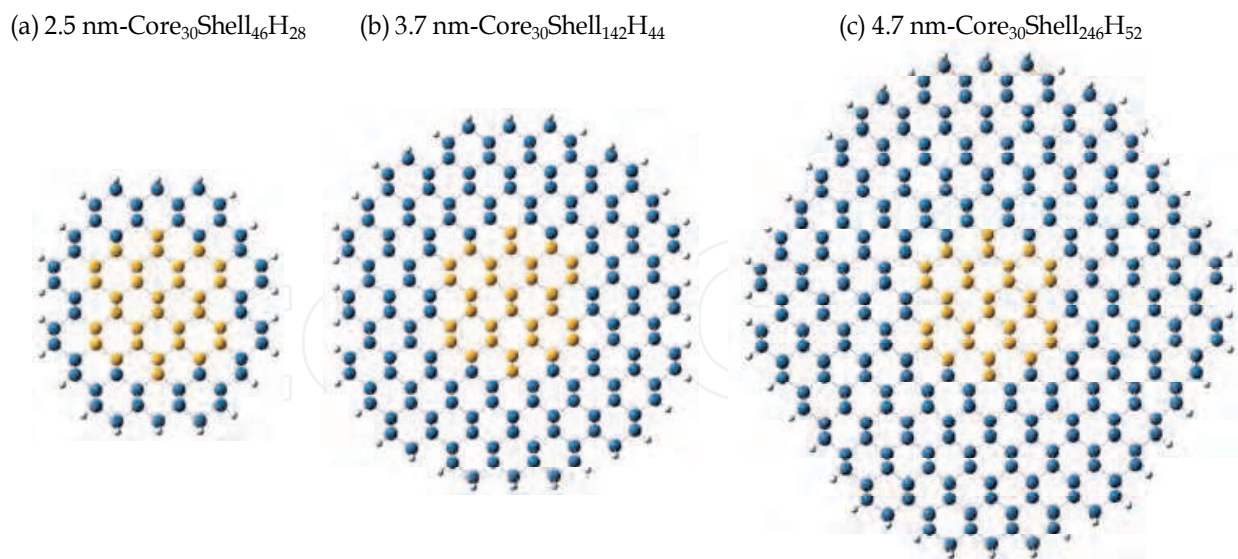
Fig. 1. Snapshots of Si/Ge core-shell nanowires viewed from the cross section. The core atoms can be Si (Ge), thus the shell will be Ge(Si). White dots on the surface are H atoms.

Dangling Si and Ge bonds on the wire surface were saturated by hydrogen atoms with the initial bond lengths 1.47 Å (Si-H), and 1.51 Å (Ge-H), respectively. Those Si-H and Ge-H bonds were allowed to relax during structure optimization. In the studied Si/Ge core-shell nanowires, the core contains 30 atoms and the thickness of the shell varies, as shown in Fig. 1. If the shell composition is Si, the initial axial lattice constant of the core-shell nanowire was set to be 0.3862 nm, taken from the lattice constant of bulk Si 0.5461 nm according to the following equation,

$$a_{\text{initial}[110]} = a_{\text{bulk}[110]} = a_{\text{bulk}} / \sqrt{2} \tag{1}$$

If the shell is Ge, the axial lattice constant was initially set to be 0.3977 nm, derived from the lattice constant of bulk Ge 0.5625 nm. We chose the initial lattice constant from the bulk shell composition since the nanowires generally have more shell atoms than core atoms (see Fig. 1). In the lateral direction of the nanowires, the vacuum distance between the wire and its mirror images (due to periodic boundary conditions) is greater than 1.0 nm, in order to eliminate the interaction between wires. The axial lattice constants of all core-shell nanowires were fully optimized through the technique of energy minimization. Atoms were fully relaxed until the forces were less than 0.02 eV/Å.

Electronic properties of a wire, such as band structure, energy gap, effective masses of charge carrier, and work function, were then calculated by solving the Kohn-Sham equation within the frame of DFT. The band gap is defined by the energy difference between the conduction band edge (CBE) and the valance band edge (VBE). The effective masses of the electron and hole can be readily calculated through parabolic fitting from the band edges according to the following formula,

$$m^* = \hbar^2 \cdot \left(\frac{d^2 E}{dk^2} \right)^{-1} \tag{2}$$

The studied Si/Ge core-shell nanowires are listed in Table 1. D is the diameter of a nanowire in unit of nanometers, defined as the longest distance between two outer shell atoms in the cross-section of the wire; N(core)/N(shell) is the number of the core/shell atoms in a given wire; N(H) is the number of H atoms needed to passivate the surface dangling bonds. Fig. 1 gives the snapshots of three core-shell nanowires with the diameters of 2.5 nm, 3.7 nm, and 4.7 nm, respectively. The diameter of the core in the nanowires is roughly 1.5 nm. The core and shell atoms could be either Si or Ge.

D (nm)	N(core)	N(shell)	N(H)
2.5	30	46	28
3.0	30	80	32
3.7	30	142	44
4.7	30	246	52

Table 1. A list of Si/Ge core-shell nanowires along the [110] direction studied in present work. D is the diameter of a wire.

Based upon the geometrically optimized wire, uniaxial tensile/compressive strain was applied by scaling the axial lattice constant. For instance, a tensile strain of 2% means that the axial lattice and the z coordinates of the atoms were rescaled to 102% of their original values, while a compressive strain of 2% implies the axial lattice and the z coordinates were rescaled to 98% of their original values. The positive values of strain refer to uniaxial expansion, while negative corresponds to compression. For each strained wire, the lateral x and y coordinates are further relaxed through energy minimization. Our study showed that the band structure of a wire is significantly modulated by strain.

2. Results and discussion

2.1 Geometrical structures of Si/Ge core-shell nanowires

The lattice constants in bulk Si and Ge are 0.5461 nm and 0.5625 nm, respectively, based on the simulation parameters mentioned above. The optimized axial lattice constants a for the Si/Ge core-shell nanowires were obtained through energy minimization. With those relaxed lattice constants, the axial stress in the wires is also minimal. The optimized lattice constants a were reported in Table 2 and Fig. 2. It shows that in the Si-core/Ge-shell nanowires, a generally increases with the diameter of the wire, from 0.3917 nm for the 2.5 nm wire to 0.3944 nm for the 4.7 nm wire. In addition, these lattice constants are smaller than 0.3977 nm (derived from bulk Ge), but larger than 0.3862 nm (derived from bulk Si), as shown in Fig. 2. These results are expected since a larger Si-core/Ge-shell wire contains more Ge atoms in the shell, thus the lattice constant generally increases with size. On the other hand, the lattice constant of the Ge-core/Si-shell nanowires decreases with the diameter of the wire, from 0.3985 nm to 0.3900 nm. It is interesting to note that the lattice constant for the smallest Ge-core/Si-shell wire with a diameter of 2.5 nm is even larger than 0.3977 nm from bulk Ge (see Fig. 2). This is consistent with the findings in pure Si and Ge nanowires with H passivation (Logan & Peng, 2009; Peng et al., 2009), in which small Si or Ge nanowires along the [110] direction were expanded, comparing to their bulk lattices.

	D (nm)	a (nm)	$\varepsilon_{\text{intrinsic}}$ to core (%)	$\varepsilon_{\text{intrinsic}}$ to shell (%)	Y (GPa)
Si-core/Ge-shell	2.5	0.3917	1.5	-1.5	67.2
	3.0	0.3945	2.2	-0.8	62.6
	3.7	0.3965	2.7	-0.3	62.3
	4.7	0.3944	2.1	-0.8	62.2
Ge-core/Si-shell	2.5	0.3985	0.2	3.2	59.2
	3.0	0.3950	-0.7	2.3	65.3
	3.7	0.3931	-1.2	1.8	67.2
	4.7	0.3900	-1.9	1.0	82.2

Table 2. The calculated structural properties in the geometrically optimized Si/Ge core-shell nanowires.

With these optimized lattice constants, an intrinsic strain was produced in the core-shell nanowires. This intrinsic strain $\varepsilon_{\text{intrinsic}}$ was calculated according to the formula,

$$\varepsilon_{\text{intrinsic}} = (a - a_{\text{bulk}[110]}) / a_{\text{bulk}[110]} \tag{3}$$

where a is the relaxed lattice constant of the nanowire, and the $a_{\text{bulk}[110]}$ is the lattice constant of bulk Si or Ge along the [110] direction. The calculated intrinsic strain was reported in Table 2. In general, the Si composition is in a tensile strain (i.e. positive strain), while the Ge composition is in a compressive strain (i.e. negative strain). This intrinsic strain brings an effect in the band gap, significantly countering the quantum confinement effect, as discussed later.
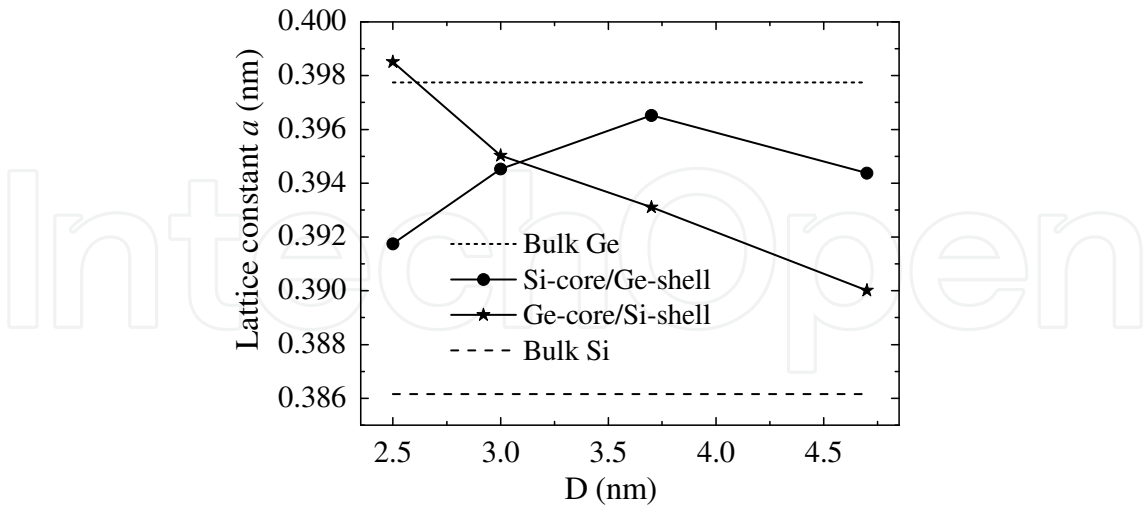

Fig. 2. The optimized axial lattice constant of Si/Ge core-shell nanowires as a function of the wire diameter.

As mentioned before, external uniaxial strain has also been applied to the geometrically relaxed nanowires. Strain energy *SE* of the nanowires is defined as the difference in the total energy between the strained and relaxed wires,

$$SE = E(total)_{strained} - E(total)_{relaxed} \qquad (4)$$

The strain energy is plotted as a function of strain in Fig. 3. From both Fig. 3(a) and 3(b), at a given value of uniaxial strain, the strain energy is greater for larger wires. For example, under -2% compression, the strain energy for the 3.0 nm Si-core/Ge-shell wire is 0.5 eV, while it is 1.3 eV for the 4.7 nm wire. Similarly, under 2% tensile strain, the strain energy for the 3.0 nm Ge-core/Si-shell wire is 0.3 eV, white it is 1.8 eV for the 4.7 nm wire. Greater strain energy in larger wires is primarily resulting from the fact that more bonds being placed under strain in the larger wires.

Young's modulus is defined as the ratio between the stress and the strain. Young's modulus of a nanostructure is dependent on its geometry, size, composition, and orientation (Xu et al., 2005; Chen et al., 2006; Lee & Rudd, 2007a, 2007b; Kulkarni et al., 2005; Liu et al., 2008). Young's modulus Y of a nanowire can be calculated from the formula,

$$Y = \frac{1}{V_0}\left(\frac{\partial^2 E}{\partial \varepsilon^2}\right)\Bigg|_{\varepsilon=0} \qquad (5)$$

where V_0 is the volume of the relaxed nanowire defined as the product of the axial lattice constant a and the cross-section area $A = \pi D^2/4$, E is the total energy, and ε is the external uniaxial strain.
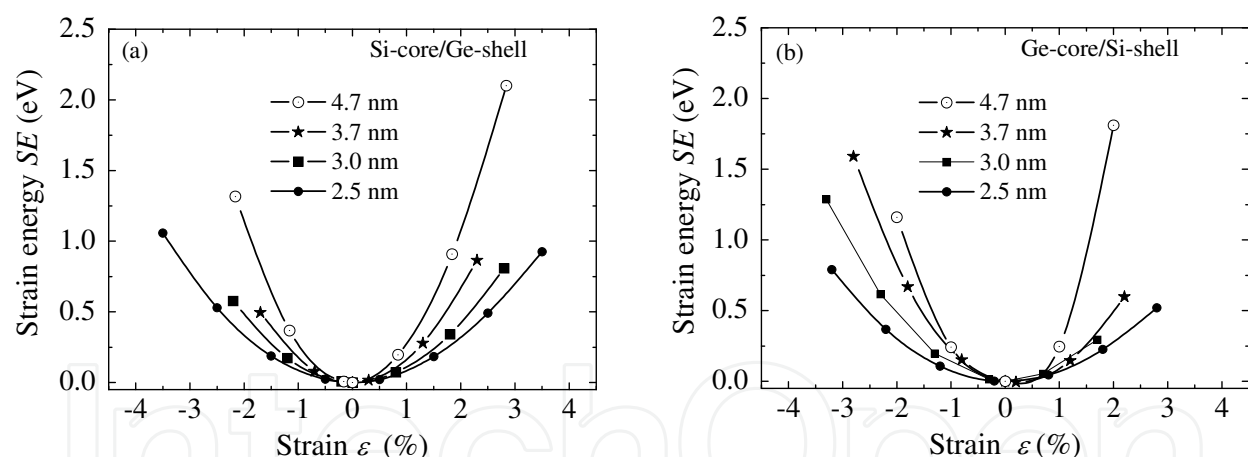

Fig. 3. The strain energies of the Si/Ge core-shell nanowires plotted as a function of strain.

The calculated modulus Y is reported in Table 2. Generally, for the Si-core/Ge-shell nanowires, the predicted Young's modulus decreases when increasing the diameter of the wire, from 67.2 GPa in the 2.5 nm wire to 62.2 GPa in the 4.7 nm wire. On the other hand, for the Ge-core/Si-shell nanowires, the Young's modulus increases with the wire diameter, from 59.2 GPa in the 2.5 nm wire to 82.2 GPa in the 4.7 nm wire. These general trends can be understood from the composition of the core-shell nanowires. Note that the Young's modulus in bulk Ge is smaller than that in bulk Si. Larger Si-core/Ge-shell nanowires contains more Ge atoms, thus a smaller modulus is expected. Similarly, larger Ge-core/Si-shell nanowires contain more Si atoms, and therefore display a larger modulus.
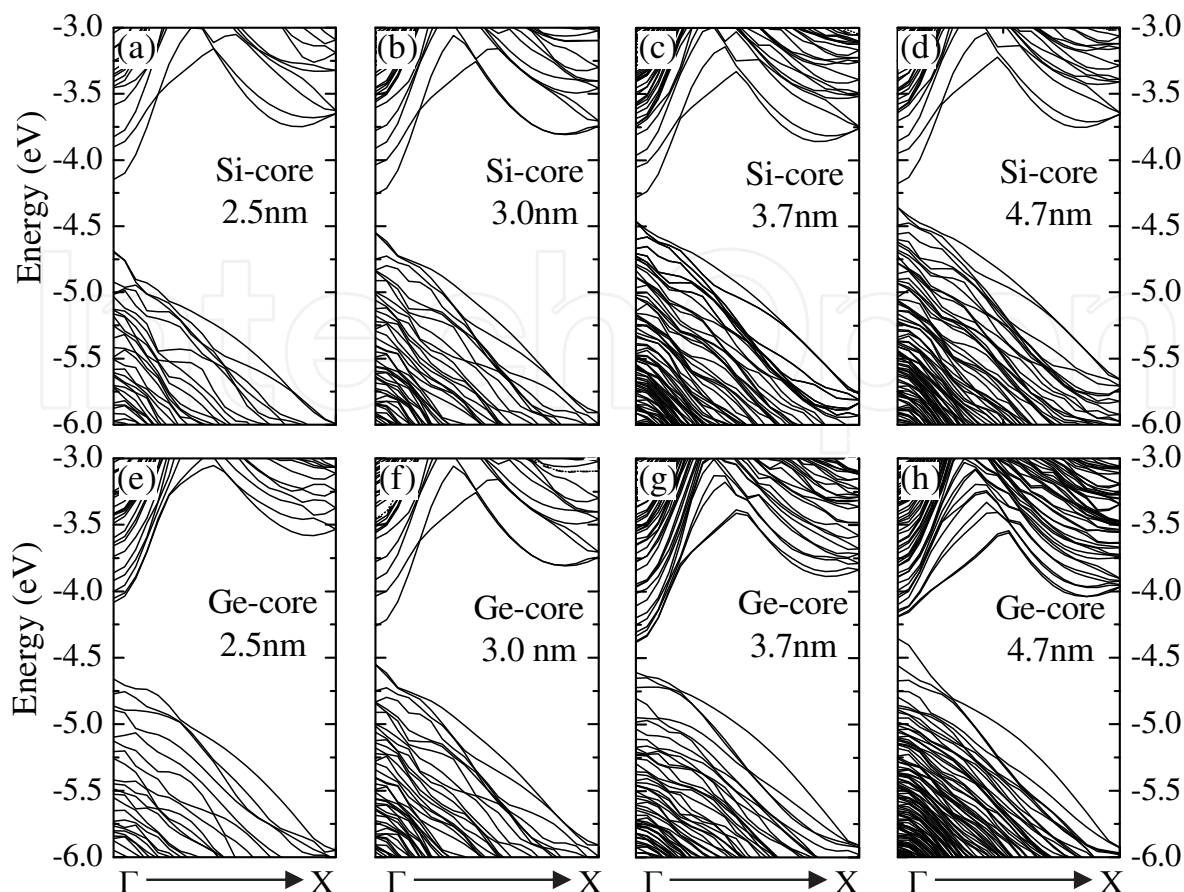
Fig. 4. The band structures of Si/Ge core-shell nanowires. The energies are referenced to the vacuum level.

3.2 Band structures
3.2.1 Band structure for relaxed Si/Ge core-shell nanowires

Bulk Si and Ge are indirect band gap materials. However, the Si/Ge core-shell and the pure Si and Ge nanowires with H passivation along the [110] direction demonstrate a direct band gap at Γ (Beckman et al., 2006; Arantes & Fazzio, 2007; Medaboina et al., 2007; L. Yang et al., 2008, Peng et al., 2009, Peng & Logan, 2010, Peng et al., 2011b). The band structures for the relaxed Si/Ge core-shell nanowires are presented in Fig. 4. In particular, the CBE and VBE were further examined, since both determine the band gap. The contour plots of charge density of CBE and VBE confirms that the band lineup in the Si/Ge core-shell nanowires is type II band offset. As an example, Fig. 5 shows the isovalue surfaces of the charge density of VBE and CBE in the nanowires with diameters of 2.5 nm and 3.7 nm. From the figures viewed in the cross sections (i.e. in the xy plane), the charge of VBE in the Si-core/Ge-shell wires is mainly distributed in the Ge shell, while the charge of CBE is mainly located in the Si core, as shown in Fig. 5(a) and 5(b). On the other hand, the charge of VBE in the Ge-core/Si-shell wires is primarily in the Ge core, while the charge of CBE is distributed in the Si shell, shown in Fig. 5(c) and 5(d). In conclusion, the VBE charge is in the Ge composition while the CBE charge is in the Si composition, regardless of whether the nanowire is of a Si-core/Ge-shell or Ge-core/Si-shell structure (L. Yang et al. 2008; Peng et al., 2011b).
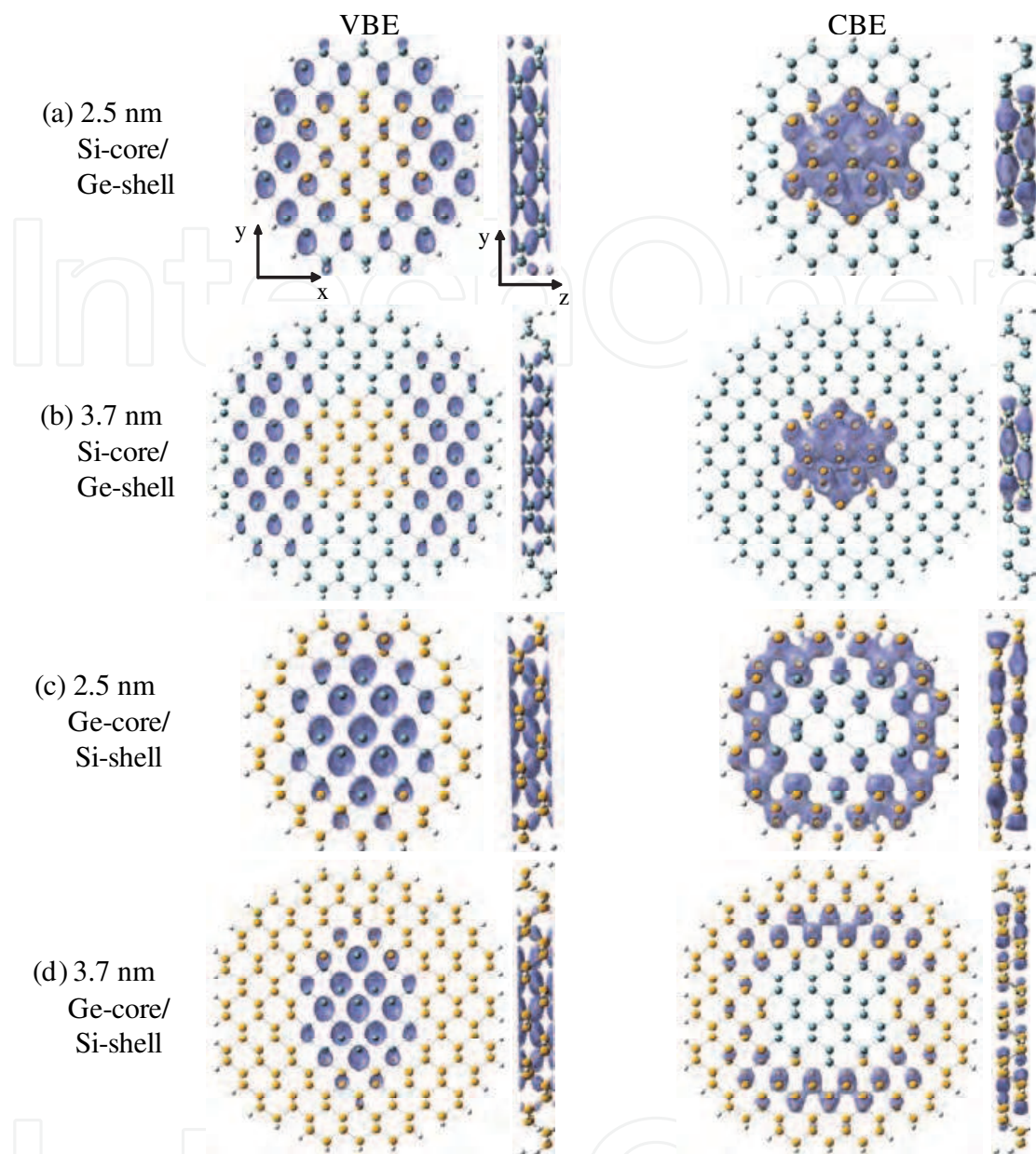
Fig. 5. The isovalue surfaces of the charge density of the valence/conduction band edges in Si/Ge core-shell nanowires. The yellow, blue and white dots represents Si, Ge, and H atoms, respectively.

This band lineup is also implied in the band structures. Examining the band edges at Γ in Fig. 4, one can notice that for the Si-core/Ge-shell wires, as shown in Fig. 4(a) – 4(d), the valence and lower occupied bands at Γ are generally close to each other, while the conduction band and higher unoccupied bands are considerably discrete. The discrete energies of the conduction band (contributed by Si composition) and neighbored unoccupied bands at Γ result from the fact that the Si atoms in the core are more significantly quantum confined compared to the Ge atoms in the shell. On the other hand, for the Ge-core/Si-shell wires in Fig. 4(e) – 4(h), the space of the energy levels in the valence band (contributed by Ge composition) and neighbored occupied bands are larger than that of conduction bands, mainly due to the fact that the Ge atoms in the core are more significantly quantum confined.

3.2.2 Band structure for strained Si/Ge core-shell nanowires

External strain shows a significant effect on the band structures of the core-shell nanowires. As an example, the band structure of 2.5 nm Ge-core/Si-shell nanowires under different values of uniaxial strain is plotted in Fig. 6(a) – 6(e). Examining the band edges, one can find that the energies of both CBE and VBE are decreased with tensile strain, while they are increased under compression. Interestingly, tensile strain shows a dramatic effect in the VBE. In Fig. 6(d) and 6(e), the VBE is no longer located at Γ, implying an indirect band gap in the nanowire. This effect and direct-to-indirect band gap transition will be discussed in detail in the following section of effective masses.
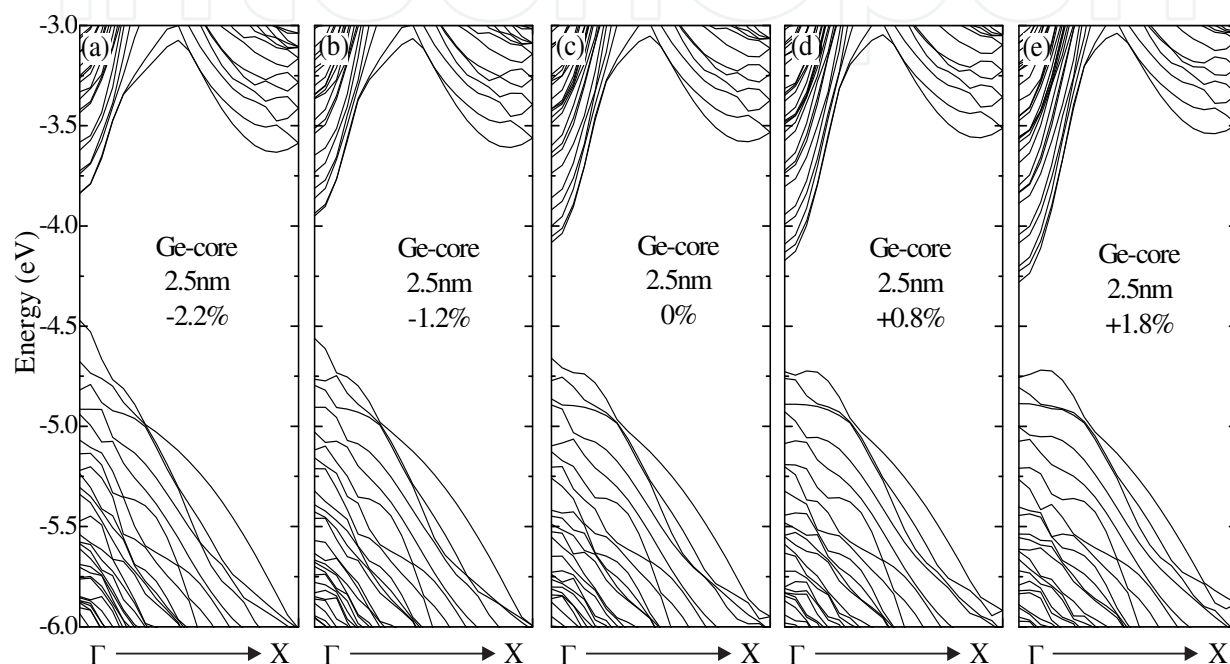

Fig. 6. The band structure of 2.5 nm Ge-core/Si-shell nanowire under different values of uniaxial strain. The energies are referenced to vacuum level.

3.3 Band gaps
3.3.1 Band gap for relaxed Si/Ge core-shell nanowires

As mentioned earlier, the band gap of the Si/Ge core-shell wire is defined by the energy difference between CBE and VBE. DFT predicted band gaps for the Si/Ge core-shell wires are given in Table 3 and Fig. 7(a). It is known that DFT underestimates the band gap of semiconductors, and an advanced GW method (Hedin, 1965; Faleev et al., 2004; Bruneval et al., 2005) can provide improved predictions. However, for the size of the nanowires investigated in the present work, GW is not applicable due to its extremely high computing cost. The present work is mainly focused on the variation of electronic properties under factors such as external strain and size. Previous studies (Peng et al., 2006) on Si nanoclusters showed that the energy gap calculated by DFT obeys a similar strain-dependency as the optical gap predicted by advanced configuration interaction (CI) method and the quasi-particle gap (defined as the difference of ionization potential and electron affinity). In addition, DFT gap predicts a similar size-dependency as the optical gap obtained using GW and quantum Monte Carlo methods (Puzder et al., 2002; Zhao et al.,

2004). Therefore, the band gap calculated by DFT should qualitatively predict the correct trends both with varying size and strain.

As shown in Fig. 7(a), the band gap of the core-shell nanowires increases with reducing wire size, which is mainly due to the quantum confinement effect. The band gaps of pure Si and Ge nanowires with H passivation are also plotted in Fig. 7(a). It is interesting to note that the band gap of the core-shell nanowires is smaller than that of both pure Si and Ge nanowires, at a given diameter. For example, the DFT gap for Si and Ge wires with the diameter 2.5 nm are 1.02 eV and 0.73 eV (Peng et al., 2009; Logan & Peng, 2009), respectively. However the gap for the Si/Ge core-shell wires are 0.58 eV(Ge-core) and 0.54 eV (Si-core), respectively, which are both smaller than that of Si and Ge wires. Similar trends are also observed for the larger wires.

	D (nm)	E_g (eV)	m_e^* (m_e)	m_h^* (m_e)	ϕ (eV)
Si-core/Ge-shell	2.5	0.54	0.13	0.16	4.64
	3.0	0.29	0.13	0.21	4.55
	3.7	0.18	0.14	0.32	4.46
	4.7	0.13	0.14	0.26	4.38
Ge-core/Si-shell	2.5	0.58	0.14	0.21	4.66
	3.0	0.31	0.13	0.17	4.58
	3.7	0.23	0.14	0.74	4.61
	4.7	0.18	0.14	0.36	4.36

Table 3. The electronic properties in the geometrically optimized Si/Ge core-shell nanowires. E_g is the band gap; m_e^* and m_h^* are the effective masses of the electron and hole in unit of free electron mass; ϕ is the work function.
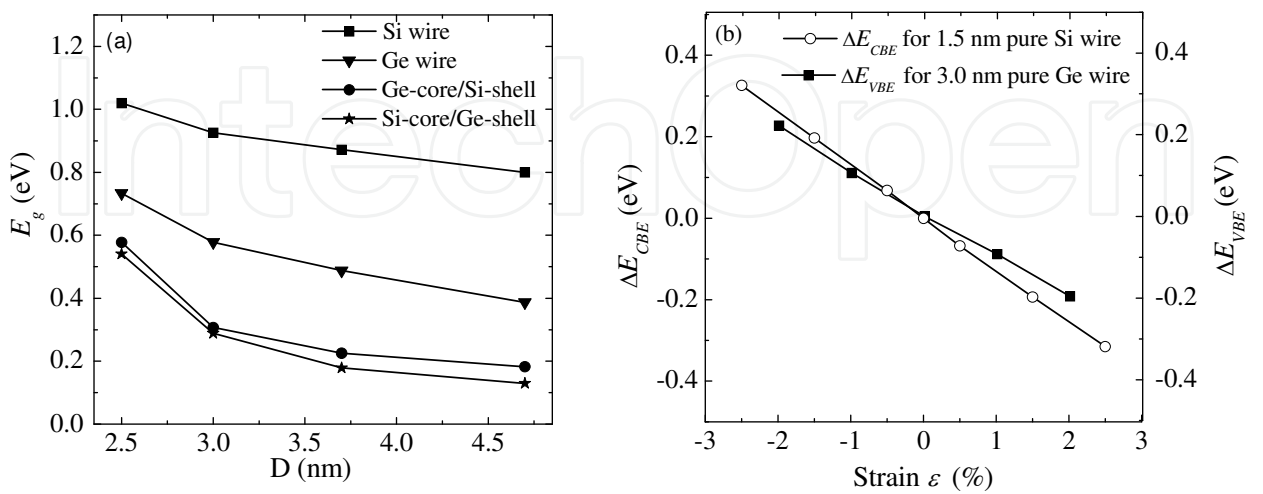

Fig. 7. (a) The band gap of Si/Ge core-shell and pure wires as a function of the wire diameter; (b) the energy variation of CBE (for 1.5 nm pure Si wire) and VBE (for 3.0 nm pure Ge wire) with strain.

In order to understand this reduced gap in the core-shell wires, the 3.0 nm Si-core/Ge-shell nanowire was examined as an example. The gap of the wire was reduced by 0.3 eV, compared to the pure 3.0 nm Ge wire. From the lattice constant and intrinsic strain reported in Table 2, the Si-core in the 3.0 nm Si-core/Ge-shell nanowire experiences a 2.2% tensile strain while the Ge-shell is contracted with a 0.8% compressive strain. Since the CBE/VBE states in the core-shell wire are primarily contributed by Si/Ge composition, we examined the CBE energy variation with strain in the pure Si nanowire of a diameter of 1.5 nm (represents the core) and the VBE energy variation with strain in the pure Ge nanowire of a diameter of 3.0 nm. The energy variations of CBE and VBE with strain is defined as,

$$\Delta E_{CBE} = E_{CBE}(\varepsilon) - E_{CBE}(0)$$
$$\Delta E_{VBE} = E_{VBE}(\varepsilon) - E_{VBE}(0)$$

(6)

where $E_{VBE}(\varepsilon)/E_{CBE}(\varepsilon)$ and $E_{VBE}(0)/E_{CBE}(0)$ are energies of VBE/CBE with and without strain, respectively. The results are shown in Fig. 7(b). The CBE of the 1.5 nm Si wire is decreased by ~ 0.28 eV under a 2.2% tensile strain. However, the VBE energy in the 3.0 nm Ge wire is increased about 0.8 eV with a 0.8% compressive strain. This implies that the band gap in the 3.0 nm Si-core/Ge-shell nanowire will be reduced by 0.36 eV, compared to the pure 3.0 nm Ge wire. This estimated reduction in the band gap (0.36 eV) is close to the actual calculation (~ 0.3 eV). Similar qualitative behaviors are also observed in the Ge-core/Si-shell nanowires.

From the above analysis, one can see that the reduced band gap is closely related to the intrinsic strain of the core-shell wires. Amato and colleagues (Amato et al., 2009) also observed a reduced band gap in Si/Ge hetero nanowires, which form an explicit interface between Si and Ge regions. The authors explained the gap reduction using quantum confinement effects in the band edges. The quantum confinement effect may be able to explain the results in their wires with diameters up to 1.6 nm. However, it is not able to explain our larger wires with a diameter up to 5 nm, where the quantum confinement is weaker. We argue that the reduction of the band gap in the Si/Ge core-shell nanowires is mainly due to the intrinsic strain in the Si/Ge composition.

3.3.2 Band gap for strained Si/Ge core-shell nanowires

The band gap of the Si/Ge core-shell nanowires can also be notably modulated by external strain. The variation of the band gap with strain is calculated as the difference in the band gap between the strained and relaxed wires,

$$\Delta E_g = E_g(\varepsilon) - E_g(0)$$

(7)

where $E_g(\varepsilon)$ and $E_g(0)$ are the band gap of the wire with and without strain, respectively. Fig. 8 plots ΔE_g as a function of uniaxial strain for the core-shell nanowires. It is clear that strain can modify the band gap. Generally, the band gap in Si/Ge core-shell nanowires decreases evidently under tensile strain, while it only slightly varies with compression. As mentioned earlier, the nanowires demonstrate a transition from a direct to indirect band gap under a sufficient tensile strain. In Fig. 8, the data points representing an indirect band gap are indicated by arrows.
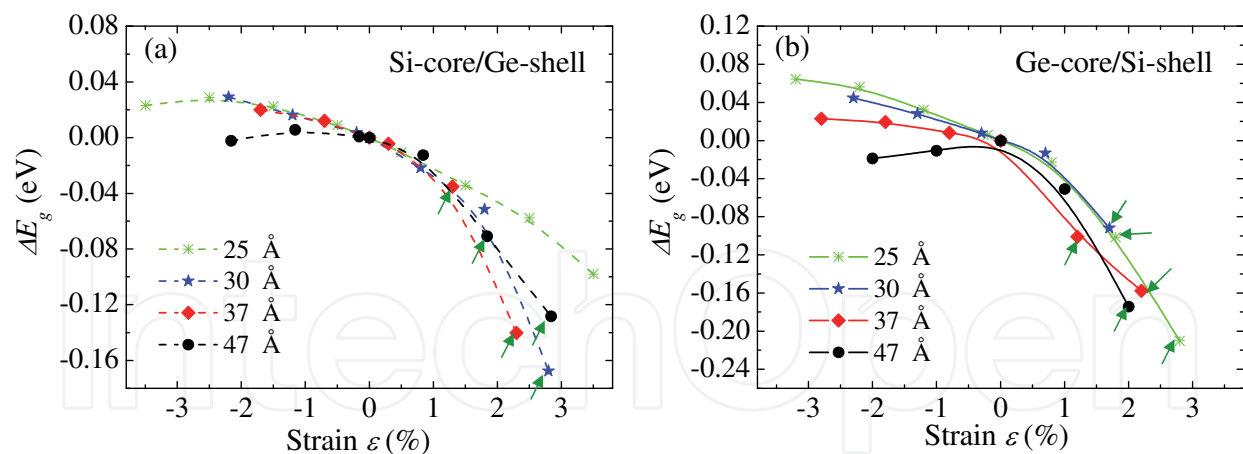
Fig. 8. The variation of the band gap in the Si/Ge core-shell wires with uniaxial strain.

In order to explain the general trends presented in Fig. 8 (i.e. the gap reducing with the uniaxial tensile strain), the energies of both CBE and VBE were further examined. The energy variation of CBE/VBE with strain is calculated as the energy difference in CBE/VBE between the strained and relaxed wires according to the equation (6). As an example, Fig. 9 shows the energy variations of CBE and VBE with strain in the 2.5 nm Si-core/Ge-shell nanowire. Note that a similar behavior is also observed for other wires. From Fig. 9, the energies of CBE and VBE both decrease nearly linearly with strain. In addition, the CBE curve has a slightly larger slope in tensile strain, compared to that of the VBE curve (thus giving a reduced gap under tensile strain).

The physical origin of the curves of the 2.5 nm Si-core/Ge-shell wire in Fig. 9 may be understandable from the wave-function character of CBE and VBE. The wave-function of various electronic states including CBE and VBE has been projected onto spherical harmonics within spheres of a radius of 1.2 Å around each Si and Ge ion. The decomposed contributions/coefficients of s, p, d orbitals are listed in Table 4. The VBE (i. e. VB at Γ) is dominated by a p_z character, which suggests that the nodal surfaces of the positive and negative values of the wave-function are perpendicular to the axis of the wire (Leu et al., 2008; Z. G. Wu et al., 2009). Under a tensile strain, the distance between the nodal surfaces increases, and the kinetic energy associated with the electron transportation between atoms reduces (Z. G. Wu et al., 2009). The same holds true for the VBE energy. For the CBE (i. e. CB at Γ), the projected wave-function includes a significant d_{z^2} character, which is consistent with literature (Richard et al., 2003; Ren et al., 1998; Filonov et al., 1995) that the d character defines the orbitals of the conduction band in a crystal. Similar to the p_z character, the d_{z^2} orbit also produces the nodal surfaces perpendicular to the axis of the wire. Therefore, the CBE energy reduces when the nanowire is under a tensile strain.

From the charge distribution of CBE and VBE shown in Fig. 5(a), one can see that the charge of VBE and CBE of the 2.5 nm Si-core/Ge-shell nanowire are mainly located in the Ge-shell and Si-core, respectively. The confined distributions of the electron charge in VBE and CBE give a clue to why the CBE curve in Fig. 9 has a larger slope compared to that of VBE curve. For the relaxed 2.5 nm Si-core/Ge-shell nanowire (i.e. no external strain applied), the intrinsic strain in the Si-core and the Ge-shell are +1.5% and -1.5%, respectively, due to the lattice mismatch of Si and Ge (Peng & Logan, 2010). If a +2% external tensile strain is applied to the wire, the resulting strain in the Si-core and Ge-shell are approximately +3.5%

and +0.5%, compared to their bulk lattice. Therefore, one expects the Si atoms in the core are more effectively expanded compared to those of the Ge atoms in the shell. Since the charge of CBE is mainly located in the Si-core while the electron of VBE is in the Ge-shell, the energy of CBE will have a larger reduction compared to that of VBE under expansion.
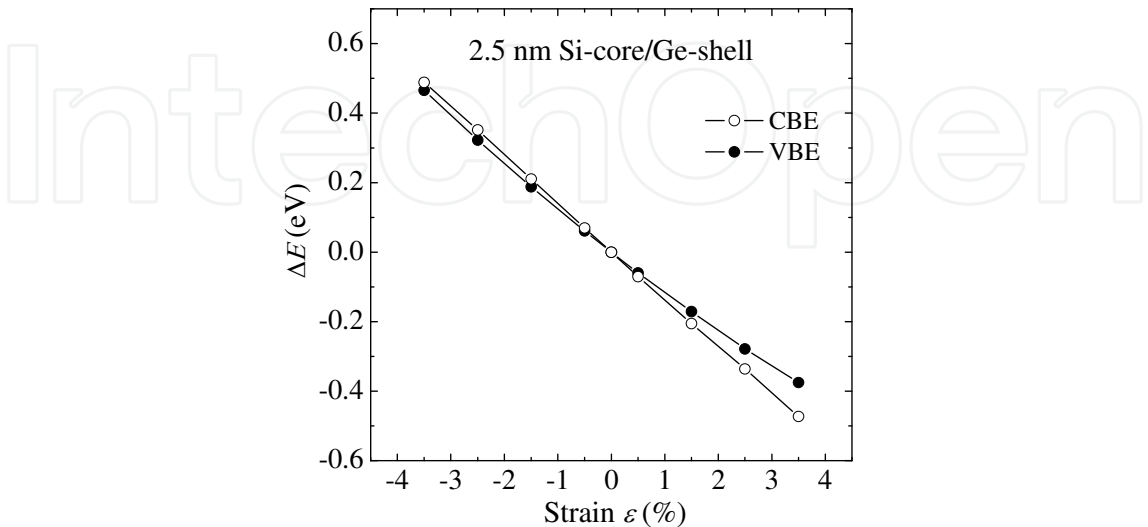

Fig. 9. The energy variation of CBE and VBE with the external strain in the Si-core/Ge-shell nanowire with the diameter of 2.5 nm. The vertical axis ΔE is defined as the energy difference of CBE/VBE between the strained and the relaxed wire.

wire	state	$|s\rangle$	$|p_x\rangle$	$|p_y\rangle$	$|p_z\rangle$	$|d_{xy}\rangle$	$|d_{yz}\rangle$	$|d_{z^2}\rangle$	$|d_{xz}\rangle$	$|d_{x^2}\rangle$
2.5 nm	VB at Γ	0.014	0.000	0.000	0.995	0.000	0.099	0.000	0.002	0.000
Si-core	VB at 0.2·2π/a	0.045	0.967	0.212	0.098	0.095	0.008	0.011	0.003	0.005
/Ge-shell	CB at Γ	0.596	0.022	0.585	0.000	0.000	0.000	0.547	0.000	0.044
	CB at 0.2·2π/a	0.603	0.155	0.532	0.054	0.012	0.006	0.066	0.006	0.567
2.5 nm	VB at Γ	0.008	0.000	0.000	0.995	0.000	0.097	0.000	0.002	0.000
Ge-core	VB at 0.2·2π/a	0.059	0.991	0.073	0.018	0.089	0.002	0.005	0.005	0.002
/Si-shell	CB at Γ	0.588	0.022	0.669	0.000	0.005	0.000	0.452	0.000	0.044
	CB at 0.2·2π/a	0.646	0.152	0.545	0.108	0.038	0.025	0.063	0.013	0.494

Table 4. Projections of the valence band (VB) and conduction band (CB) onto the s, p, and d states in the 2.5 nm Si/Ge core-shell nanowires.

3.4 Effective masses of electron and hole
3.4.1 Effective masses of electron and hole for relaxed Si/Ge core-shell nanowires
The effective masses of the electron and hole can be obtained from the band structure of the nanowires according to equation (2) through parabolic fitting the band edges. The calculated effective masses of the electron and hole for the relaxed Si/Ge core-shell nanowires are reported in Table 3, where m_e^* represents the effective mass of the electron, while m_h^* is the effective mass of the hole, in unit of free electron mass m_e. The effective mass of the electron are 0.13 m_e or 0.14 m_e, having a negligible change with size and the core-shell composition. In contrast, the effective mass of the hole is dependent on the wire size and composition.

3.4.2 Effective masses of electron and hole for the strained Si/Ge core-shell nanowires

The strain effect on the effective masses of the electron and hole were further studied. Taking the 2.5 nm Ge-core/Si-shell wire as an example, the dispersion relation with the K vector in the range of ±0.2·b, where $b = 2\pi/a$, is plotted under different values of strain in Fig. 10(a). It shows that strain has a dominant effect on the band structure at Γ - the energies are evidently shifted (Peng et al., 2011b). However, the strain has a negligible effect on the bands with K vectors away from Γ (K > 0.15· b or K < -0.15· b). These strain effects may be understandable from a simple tight-binding model discussed in the reference (Logan & Peng, 2009). For an in-depth understanding, a detailed analysis of the wave-function character is reported in Table 4. For the valence/conduction band at Γ, there is a significant portion of p_z/d_{z^2} character. Therefore, the energy of the valence/conduction band at Γ decreases with an external tensile strain (see details discussion on Fig. 9). However, for the wave-functions at K = 0.20· b, the portion of p_z/d_{z^2} character is largely reduced, while the p_x/p_y character dominates. With the p_x/p_y character, the nodal surfaces of the wave-functions are parallel to the axis of the nanowire and the distance between the nodal surfaces is negligibly changed by a uniaxial strain. Therefore, the kinetic energy associated with the electron transportation stays the same, giving a minimal energy shift with strain (Z. G. Wu et al., 2009).
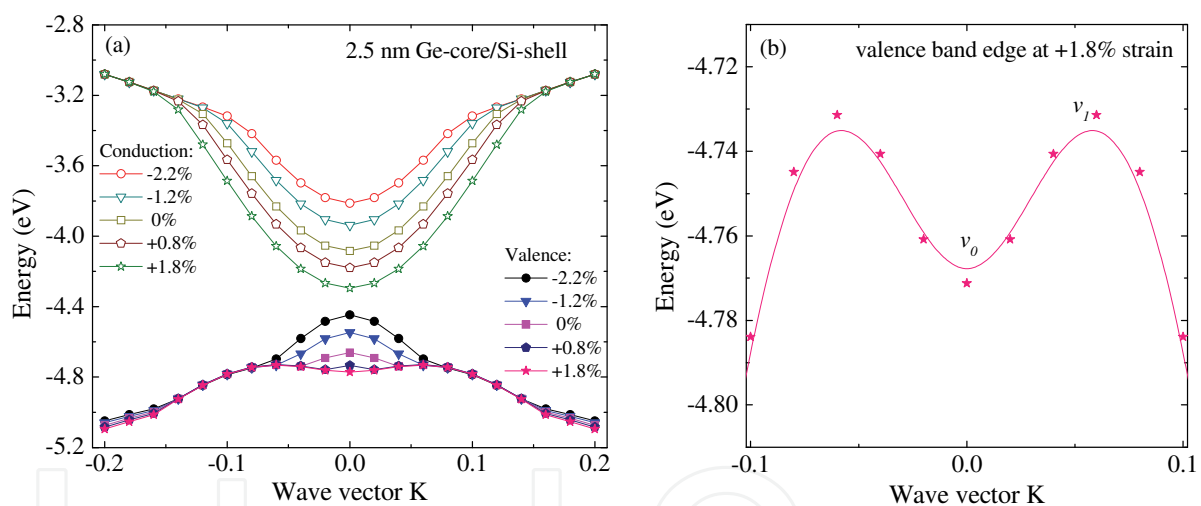

Fig. 10. The conduction and valence band of a Ge-core/Si-shell wire with a diameter of 2.5 nm at the near region of Γ under different values of uniaxial strain. The curve of valence band under +1.8% strain has been enlarged in (b), indicating an indirect band gap with valence band egde located at state v_1 rather than v_0.

From Fig. 10(a), the CBE is located at Γ, regardless of the values of uniaxial strain. However, the VBE shows an interesting transition – it is no longer located at Γ for a large tensile strain (+1.8%), implying an indirect band gap. An enlarged graph of the VBE under +1.8% strain is presented in Fig. 10(b). The nature of the band gap (direct or indirect) is determined by the energies of the two states labeled as v_0 at Γ and v_1 at K = 0.05· b. Without strain, the energy of v_0 is higher than that of v_1, as shown in Fig. 10(a), resulting in a direct band gap. With +1.8% tensile strain, the energy of v_1 is higher than that of v_0, giving an indirect band gap.

This direct-to-indirect gap transition with strain is clearly demonstrated in Fig. 10. In Fig. 10(a), the energy of the valence band at Γ (K = 0.0) is noticeably decreased with tensile

strain, where the energy shift of the valence band at K vectors away from Γ (i.e. K > 0.05·*b*) is negligible with strain. Therefore, with a sufficient tensile strain, the energy of the valence band at Γ can be reduced to an extent so that it is lower than the energy at K = 0.05· *b*. The reason for the different band energy shifts at Γ and other K vectors with strain stems from their different *s*, *p*, *d* orbital projection. (See the above section for detailed discussion).

The strain effects on the effective masses of the electron and hole are reported in Fig. 11. The variation of the effective mass of the electron with strain for three wires with a diameter of 2.5 nm, 3.0 nm and 3.7 nm are minimal, as shown in Fig. 11(a) and 11(b). For the wire with a diameter of 4.7 nm, the effective mass of the electron slightly increases with the compressive strain. In contrast, the change in the effective mass of the hole is dramatic, as shown in Fig. 11(c) and 11(d). Taking the 2.5 nm Ge-core/Si-shell wire as an example, the effective mass of the hole decreases from 0.21 m_e (no strain) to 0.15 m_e (-2.2% strain), which is indicated by the dispersion relations in Fig. 10(a) shown by the curves with solid dots and squares, respectively. In the case of the 3.0 nm Ge-core/Si-shell wire, the effective mass of the hole decreases slightly from 0.166 m_e without strain to 0.145 m_e at -2.3% strain (decreased by 13%), while it dramatically increases to 0.728 m_e at 0.7% tensile strain (increased ~ 300%). When a +1.7% tensile strain is applied, the VBE of the wire shifts from Γ to the K vector at 0.04· b. The effective mass of the hole was reduced back to 0.453 m_e by a parabolic fitting of the dispersion relation near this new K vector. Similar behavior is also observed for other wires, as shown in Fig. 11(c) and 11(d).
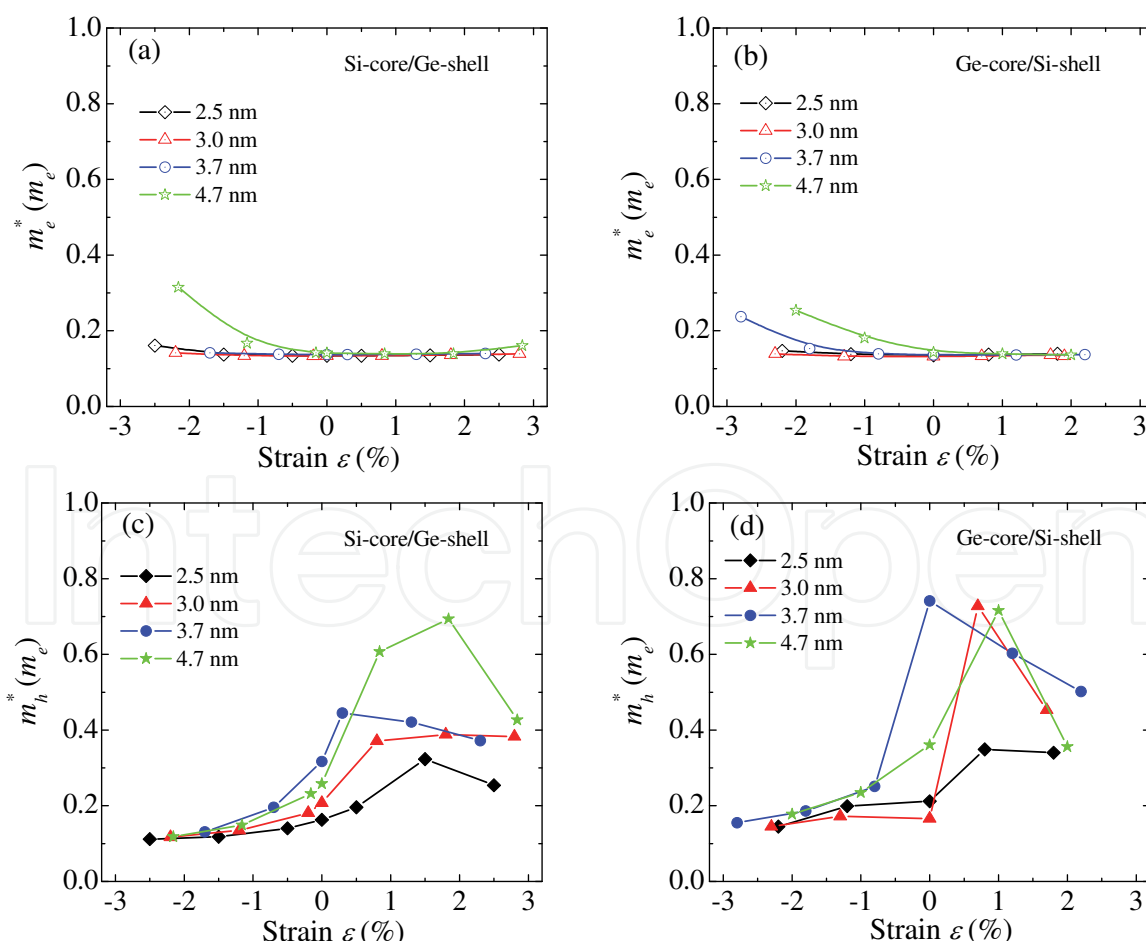

Fig. 11. The effective masses of the electron and hole as a function of strain for Si/Ge core-shell nanowires at different size and composition.

It is concluded that the effective mass of the hole in the Si/Ge core-shell nanowires is much more sensitive to strain, compared to that of the electron. This is also implied in Fig. 10(a), in which the curvature of the conduction band around Γ is not sensitive to strain. However, the shape of the valence band is dramatically changed with strain.

3.5 Work function
3.5.1 Work function of the relaxed Si/Ge core-shell nanowires
It is of great importance to predict work function of semiconducting nanowires, since it affects band alignment in nanowire/metal interfaces and displays impact in device performance (Leu et al., 2008). The work function of a nanowire is defined as the energy difference between Fermi and vacuum levels,

$$\phi = V_{vacuum} - E_{Fermi} \qquad (8)$$

Usually in first principles DFT calculations, the Fermi level is set to be the energy level of the highest occupied state, i. e. VBE. Since all electronic energies in present calculations are referenced to the vacuum, the work function ϕ is simply,

$$\phi = -E_{VBE} \qquad (9)$$

The calculated work functions ϕ for the Si/Ge core-shell nanowires are reported in Table 3. The work function is in the range of 4.4 ~ 4.6 eV, consistent with the reported work function of H-passivated Si nanowires along the [110] direction (Ng et al., 2010; Leu et al., 2008). In general, the work function of the nanowire decreases with increasing size. For example, the work function of the Si-core/Ge-shell nanowires reduces from 4.64 eV for the 2.5 nm wire to 4.38 eV for the 4.7 nm. For the Ge-core/Si-shell wires, it decreases from 4.66 eV in 2.5 nm wire to 4.36 eV in 4.7 nm wire. This general trend is also demonstrated in the band structures in Fig. 4. Since the band energies in Fig. 4 are reference to vacuum level, the energy of VBE reflects the work function (with opposite sign). With increasing nanowire size, the VBE energies increase, implying that the work function decreases. This size-dependence of the work function is also consistent with that of Si nanowires (Ng et al., 2010; Leu et al., 2008).
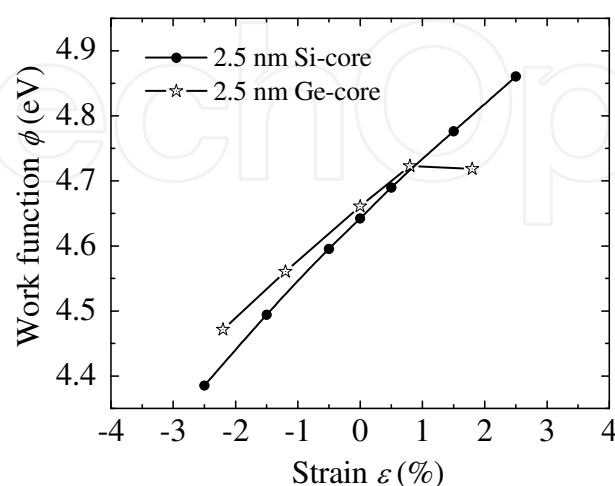

Fig. 12. The work function of the 2.5 nm Si/Ge core-shell nanowires as a function of external uniaxial strain.

3.5.2 Work function of the strained Si/Ge core-shell nanowires

It was also found that the work function of the Si/Ge core-shell nanowires can be modulated by external uniaxial strain. As an example, Fig. 12 presents the variation of the work function with strain in the 2.5 nm Si/Ge core-shell nanowires. In general, the work function for both wires increases with tensile strain, while reduces under compression. The effect was discussed in details in the above section for Fig. 10 and Fig. 7(b), where the energy of VBE is decreasing with tensile strain (note that the change of the potential of vacuum level is negligible with strain). This general trend is consistent with that in Si nanowires (Leu et al., 2008) and graphene nanoribbons (Peng et al., 2011a). In addition, it is interesting to note that the work function of the Si-core/Ge-shell wire increases nearly linearly, whereas for the Ge-core/Si-shell wire it saturates at a value on the tensile train (shown in Fig. 12). This is due to the fact that with the tensile strain, the VBE of the Ge-core/Si-shell nanowires is located at $K = 0.075 \cdot b$, rather than at Γ and shifts negligible with strain (see Fig. 6 and Fig. 10).

4. Conclusion & future work

In summary, first principles DFT calculations were performed to study the structural, mechanical and electronic properties of Si/Ge core-shell nanowires with the diameter up to 5 nm. Firstly, it was found that an intrinsic strain was produced in the core-shell nanowires. The intrinsic strain shows a dramatic effect in reduction of the band gap in the core-shell structure, significantly countering the quantum confinement effect. Secondly, the band structure can be greatly modified by external uniaxial strain, therefore the electronic properties, such as the band gap, effective masses of the electron and hole, work function, can be modulated by the strain.

The Si/Ge core-shell nanowires were demonstrated with a type II band alignment, where the valence band is contributed by Ge composition, while the conduction band is contributed by Si composition. In this case, electrons and holes are separated into core and shell regions, respectively. This offers an opportunity to employ the core-shell structure for novel device applications. To fulfill the purpose, an appropriate doping strategy has to be developed. We propose to theoretically investigate the effects of defects and surface functionality on the electronic properties of core-shell nanowires. Particularly, the shallow states introduced near VBE/CBE need be thoroughly studied, which potentially serve as the donor/acceptor centers. In addition, a dispersed/alloyed Si and Ge nanowire is also of great interest to study, bridging the knowledge of pure and core-shell nanowires. The dispersed/alloyed nanowires yield a maximum Si/Ge interface, where novel electronic properties could occur.

5. Acknowledgement

6. References

Amato M, Palummo M & Ossicini S, (2009) Reduced quantum confinement effect and electron-hole separation in SiGe nanowires, *Phys. Rev. B* 79 201302- 201305

Arantes J T & Fazzio A, (2007) Theoretical investigations of Ge nanowires grown along the [110] and [111] directions, *Nanotechnology* 18 295706-295710

Audoit G, Ni Mhuircheartaigh T, Lipson S M, Morris M A, Blau W J & Holmes J D, (2005) Strain induced photoluminescence from silicon and germanium nanowire arrays, *J. Mater. Chem.* 15 4809-4815

Beckman S P, Han J & Chelikowsky J R, (2006) Quantum confinement effects in Ge [110] nanowires, *Phys. Rev. B* 74 165314-165318

Bruneval F, Sottile F, Olevano V, Del Sole R & Reining L, (2005) Many-body perturbation theory using the density-functional concept: Beyond the GW approximation, *Phys. Rev. Lett.* 94 186402-186405

Bruno M, Palummo M, Marini A, Del Sole R, Olevano V, Kholod A N & Ossicini S, (2005) Excitons in germanium nanowires: Quantum confinement, orientation, and anisotropy effects within a first-principles approach, *Phys. Rev. B* 72 153310-153313

Chen C Q, Shi Y, Zhang Y S, Zhu J & Yan Y J, (2006) Size Dependence of Young's Modulus in ZnO Nanowires, *Phys. Rev. Lett.* 96 075505

Cui Y & Lieber C M, (2001) Functional nanoscale electronic devices assembled using silicon nanowire building blocks, *Science* 291 851-853

Cui Y, Wei Q Q, Park H K & Lieber C M, (2001) Nanowire nanosensors for highly sensitive and selective detection of biological and chemical species, *Science* 293 1289-1292

Cui Y, Zhong Z H, Wang D L, Wang W U & Lieber C M, (2003) High performance silicon nanowire field effect transistors, *Nano Lett.* 3 149-152

Dailey E & Drucker J, (2009) "Seedless" vapor-liquid-solid growth of Si and Ge nanowires: The origin of bimodal diameter distributions, *J. Appl. Phys.* 105 064317-064321

Faleev S V, van Schilfgaarde M & Kotani T, (2004) All-electron self-consistent GW approximation: Application to Si, MnO, and NiO, *Phys. Rev. Lett.* 93 126406-126409

Filonov A B, Tralle I E, Petrov G V & Borisenko V E, (1995) Silicon band-structure calculations by the self-consistent crystalline orbital method *Modell. Simul. Mater. Sci. Eng* 3 45-52

Goldthorpe I A, Marshall A F & McIntyre P C, (2008) Synthesis and strain relaxation of Ge-core/Si-shell nanowire arrays, *Nano Lett.* 8 4081-4086

Hahm J & Lieber C M, (2004) Direct ultrasensitive electrical detection of DNA and DNA sequence variations using nanowire nanosensors, *Nano Lett.* 4 51-54

Hedin L, (1965) New method for calculating the one-particle Green's function with application to the electron-gas problem, *Phys. Rev.* 139 A796-A823

Hirschman K D, Tsybeskov L, Duttagupta S P & Fauchet P M, (1996) Silicon-based visible light-emitting devices integrated into microelectronic circuits, *Nature* 384 338-341

Holmes J D, Johnston K P, Doty R C & Korgel B A, (2000) Control of thickness and orientation of solution-grown silicon nanowires, *Science* 287 1471-1473

Hu B Y-K & Das Sarma S, (1992) Many-body properties of a quasi-one-dimensional semiconductor quantum wire, *Phys. Rev. Lett.* 68 1750-1753

Hu J Q, Bando Y & Golberg D, (2009) Novel semiconducting nanowire heterostructures: Synthesis, properties and applications, *J. Mater. Chem.* 19 330-343

Hu Y J, Xiang J, Liang G C, Yan H & Lieber C M, (2008) Sub-100 nanometer channel length Ge/Si nanowire transistors with potential for 2 THz switching speed, *Nano Lett.* 8 925-930

Kagimura R, Nunes R W & Chacham H, (2007) Surface dangling-bond states and band lineups in hydrogen-terminated Si, Ge, and Ge/Si nanowires, *Phys. Rev. Lett.* 98 026801- 026805

Kohn W & Sham L J, (1965) Self-consistent equations including exchange and correlation effects, *Phys. Rev.* 140 1133-1138

Koo S M, Fujiwara A, Han J P, Vogel E M, Richter C A & Bonevich J E, (2004) High inversion current in silicon nanowire field effect transistors, *Nano Lett.* 4 2197-2201

Kresse G & Furthmuller J, (1996) Efficiency of ab-initio total energy calculations for metals and semiconductors using a plane-wave basis set, *Comput. Mater. Sci.* 6 15-50

Kresse G & Furthmuller J, (1996) Efficient iterative schemes for ab initio total-energy calculations using a plane-wave basis set, *Phys. Rev. B* 54 11169-11186

Kulkarni A J, Zhou M & Ke F J, (2005) Orientation and size dependence of the elastic properties of zinc oxide nanobelts, *Nanotechnology* 16 2749-2756

Lauhon L J, Gudiksen M S, Wang C L & Lieber C M, (2002) Epitaxial core-shell and core-multishell nanowire heterostructures, *Nature* 420 57-61

Lee B & Rudd R E, (2007) First-principles calculation of mechanical properties of Si<001> nanowires and comparison to nanomechanical theory, *Phys. Rev. B* 75 195328-195340

Lee B & Rudd R E, (2007) First-principles study of the Young's modulus of Si<001> nanowires, *Phys. Rev. B* 75 041305-041308

Leu P W, Svizhenko A & Cho K, (2008) Ab initio calculations of the mechanical and electronic properties of strained Si nanowires, *Phys. Rev. B* 77 235305-235318

Liu X W, Hu J & Pan B C, (2008) The composition-dependent mechanical properties of Ge/Si core-shell nanowires, *Physica E: Low-dimensional Systems and Nanostructures* 40 3042-3048

Logan P & Peng X H, (2009) Strain-modulated electronic properties of Ge nanowires: A first-principles study, *Phys. Rev. B* 80 115322-115328

Lu W, Xiang J, Timko B P, Wu Y & Lieber C M, (2005) One-dimensional hole gas in germanium/silicon nanowire heterostructures, *Proc. Natl. Acad. Sci. U. S. A.* 102 10046-10051

Medaboina D, Gade V, Patil S K R & Khare S V, (2007) Effect of structure, surface passivation, and doping on the electronic properties of Ge nanowires: A first-principles study, *Phys. Rev. B* 76 205327-2053213

Migas D B & Borisenko V E, (2007) Structural, electronic, and optical properties of <001>-oriented SiGe nanowires, *Phys. Rev. B* 76 035440-035448

Morales A M & Lieber C M, (1998) A laser ablation method for the synthesis of crystalline semiconductor nanowires, *Science* 279 208-211

Musin R N & Wang X Q, (2005) Structural and electronic properties of epitaxial core-shell nanowire heterostructures, *Phys. Rev. B* 71 155318-155321

Musin R N & Wang X Q, (2006) Quantum size effect in core-shell structured silicon-germanium nanowires, *Phys. Rev. B* 74 165308-165312

Ng M F, Sim L Y, Da H X, Jin H M, Lim K H & Yang S W, (2010) Modulation of the work function of silicon nanowire by chemical surface passivation: a DFT study, *Theoretical Chemistry Accounts* 127 689-695

Peelaers H, Partoens B & Peeters F M, (2007) Properties of B and P doped Ge nanowires, *Appl. Phys. Lett.* 90 263103-263105

Peng X H, Alizadeh A, Kumar S K & Nayak S K, (2009) Ab-initio study of size and strain effects on the electronic properties of Si nanowires, *Int. J. of Applied Mechanics* 1 483-499

Peng X H, Ganti S, Alizadeh A, Sharma P, Kumar S K & Nayak S K, (2006) Strain-engineered photoluminescence of silicon nanoclusters, *Phys. Rev. B* 74 035339-035343

Peng X H & Logan P, (2010) Electronic properties of strained Si/Ge core-shell nanowires, *Appl. Phys. Lett.* 96 143119-143121

Peng X H, Tang F & Copple A, (2011) Work function of armchair graphene nanoribbons, (unpublished)

Peng X H, Tang F & Logan P, (2011) Band structure of Si/Ge core-shell nanowires along [110] direction modulated by external uniaxial strain, *J. Phys. Condens. Matter* 23, 115502-115509

Puzder A, Williamson A J, Grossman J C & Galli G, (2002) Surface chemistry of silicon nanoclusters, *Phys. Rev. Lett.* 88 097401-097404

Ren S Y, Chen X & Dow J D, (1998) Tight-binding sp^3d^5 Hamiltonian for Si, *J. Phys. Chem. Solids* 59 403-410

Richard S, Aniel F, Fishman G & Cavassilas N, (2003) Energy-band structure in strained silicon: A 20-band k-p and Bir-Pikus Hamiltonian model, *J. Appl. Phys.* 94 1795-1799

Tian B Z, Zheng X L, Kempa T J, Fang Y, Yu N F, Yu G H, Huang J L & Lieber C M, (2007) Coaxial silicon nanowires as solar cells and nanoelectronic power sources, *Nature* 449 885-889

Trammell T E, Zhang X, Li Y L, Chen L Q & Dickey E C, (2008) Equilibrium strain-energy analysis of coherently strained core-shell nanowires, *J. Cryst. Growth* 310 3084-3092

Vanderbilt D, (1990) Soft self-consistent pseudopotentials in a generalized eigenvalue formalism, *Phys. Rev. B* 41 7892-7895

Varahramyan K M, Ferrer D, Tutuc E & Banerjee S K, (2009) Band engineered epitaxial Ge-Si_xGe_{1-x} core-shell nanowire heterostructures, *Appl. Phys. Lett.* 95 033101-033103

Wu X Y, Kulkarni J S, Collins G, Petkov N, Almecija D, Boland J J, Erts D & Holmes J D, (2008) Synthesis and electrical and mechanical properties of silicon and germanium nanowires, *Chem. Mat.* 20 5954-5967

Wu Y Y, Fan R & Yang P D, (2002) Block-by-block growth of single-crystalline Si/SiGe superlattice nanowires, *Nano Lett.* 2 83-86

Wu Z, Neaton J B & Grossman J C, (2008) Quantum confinement and electronic properties of tapered silicon nanowires, *Phys. Rev. Lett.* 100 246804-246807

Wu Z G, Neaton J B & Grossman J C, (2009) Charge separation via strain in silicon nanowires, *Nano Lett.* 9 2418-2422

Xu B, Lu A J, Pan B C & Yu Q X, (2005) Atomic structures and mechanical properties of single-crystal GaN nanotubes, *Phys. Rev. B* 71 125434-125439

Yang J E, Jin C B, Kim C J & Jo M H, (2006) Band-gap modulation in single-crystalline $Si_{1-x}Ge_x$ nanowires, *Nano Lett.* 6 2679-2684

Yang L, Musin R N, Wang X Q & Chou M Y, (2008) Quantum confinement effect in Si/Ge core-shell nanowires: First-principles calculations, *Phys. Rev. B* 77 195325- 195329

Zhao X, Wei C M, Yang L & Chou M Y, (2004) Quantum confinement and electronic properties of silicon nanowires, *Phys. Rev. Lett.* 92 236805-236808

Nanowires - Fundamental Research

Edited by Dr. Abbass Hashim

Understanding and building up the foundation of nanowire concept is a high requirement and a bridge to new technologies. Any attempt in such direction is considered as one step forward in the challenge of advanced nanotechnology. In the last few years, InTech scientific publisher has been taking the initiative of helping worldwide scientists to share and improve the methods and the nanowire technology. This book is one of InTech's attempts to contribute to the promotion of this technology.

How to reference

In order to correctly reference this scholarly work, feel free to copy and paste the following:

Xihong Peng, Fu Tang and Paul Logan (2011). First Principles Study of Si/Ge Core-Shell Nanowires ---- Structural and Electronic Properties, Nanowires - Fundamental Research, Dr. Abbass Hashim (Ed.), ISBN: 978-953-307-327-9, InTech, Available from: http://www.intechopen.com/books/nanowires-fundamental-research/first-principles-study-of-si-ge-core-shell-nanowires-structural-and-electronic-properties

INTECH
open science | open minds